Progress In Electromagnetics Research C, Vol. 173, 167–179, 2026

PIER C

(Received 1 July 2026, Accepted 13 August 2026, Scheduled 6 September 2026)

A Compact Fibonacci Fractal MIMO Antenna with Slotted Decoupling Structure for 5G and WLAN Applications

Sachin S. Khade[1,*], Nikhil Mangrulkar[2,*], Praful N. Yerkewar[3], Tirupati M. Goskula[4], Chitra S. Khade[5], and Prajwal Rewatkar[1]

[1] *Yeshwantrao Chavan College of Engineering, Nagpur, India*
[2] *Symbiosis Institute of Technology Nagpur Campus, Symbiosis International (Deemed University), Pune, India*
[3] *PBCOE, Nagpur, India*
[4] *Anjuman College of Engineering & Technology Nagpur, India*
[5] *GHRCEM, Nagpur, India*

ABSTRACT: A miniaturized, multiband, Fibonacci-inspired MIMO antenna is proposed for modern wireless communication technologies, such as sub-6 GHz 5G, WiMAX, WLAN, and Wi-Fi. The proposed antenna incorporates a Fibonacci spiral as the radiating element along with an enhanced defected ground structure (DGS). This configuration provides improved impedance matching, low mutual coupling, and strong diversity characteristics. The antenna employs a slot-loaded decoupling strip and an optimized ground plane to suppress surface currents and enhance isolation between elements. In its final two-element configuration, the antenna exhibits three distinct resonant frequencies at 1.1 GHz, 4.22 GHz, and 5.65 GHz. Both simulated and measured results demonstrate excellent impedance matching, achieving a minimum return loss of -27.22 dB at 4.22 GHz and an isolation level better than -20 dB throughout the operating frequency range. Moreover, the envelope correlation coefficient (ECC) remains below 0.05, while the diversity gain exceeds 9.95 dB. The antenna also achieves a radiation efficiency ranging from 75% to 85%. Surface current analysis further demonstrates that the combination of the Fibonacci-inspired geometry and DGS effectively produces multiband operation while minimizing mutual coupling.

1. INTRODUCTION

New emerging trends from 2024 to 2026 highlight the importance of miniaturization, a high level of isolation, and multiband or wideband capabilities in compact 5G antennas. Recent studies show that fractal-based multiple-input multiple-output (MIMO) antennas are viable solutions for meeting the strict demands of next-generation wireless communication systems. For example, a Hilbert curve fractal MIMO slot antenna optimized with a genetic algorithm achieved good impedance bandwidth, solid isolation, stable radiation characteristics, and a low ECC for Wi-Fi 7 and Wi-Fi 8 applications [1, 2]. Fractal geometries effectively improve antenna bandwidth, isolation, and radiation performance; however, further enhancements in compactness and multiband operation are still active research challenges [3].

Notable examples include fractal Hilbert MIMO antennas, miniaturized multiband MIMO antennas using DGS [4], and compact fractal MIMO designs incorporating stubs and notches [5]. Advanced four-element and four-port MIMO architectures have also been reported, achieving high isolation for next-generation wireless applications [6–8]. Fractal antennas designed for ultra-wideband and multiband MIMO have shown great effectiveness in bandwidth and diversity [9, 10]. To improve isolation and impedance characteristics, many designs use space-filling fractal geometries along with defected ground structures, parasitic elements, and multi-port configurations [1–12]. Despite significant advancements, several limitations still exist. First, many existing designs rely on multiple decoupling mechanisms simultaneously — such as combining DGS with stubs, slots, or parasitic elements — which increases structural complexity and fabrication sensitivity [5–8, 12]. Second, although four-element and higher-order MIMO antennas have been reported [6, 10, 13], systematic scalability analysis is limited, with most studies validating only a single configuration of the antenna. Third, comparative benchmarking across sub-6 GHz, ultra-wideband (UWB), and FR2 bands is scarce, hindering the assessment of a unified fractal topology across multiple 5G frequency ranges [9, 11, 14]. Moreover, physical insight into isolation mechanisms is often qualitative, with limited use of characteristic mode or surface current analysis [13]. Finally, compactness, isolation, and radiation efficiency are rarely optimized jointly, as many miniaturized designs achieve isolation at the expense of efficiency or gain [1, 5, 10].

With the evolution of 5G New Radio (NR), research has been extended toward higher-order MIMO arrays and millimeter-wave frequencies. Fractal-loaded two- and eight-element MIMO antennas have been proposed for sub-6 GHz 5G and WLAN applications, with characteristic mode analysis employed to explain isolation mechanisms [13]. Furthermore, modified spherical and Minkowski fractal geometries have

* Corresponding authors: Sachin S. Khade (sac_mob@rediffmail.com); Nikhil Mangrulkar (mangrulkar.nikhil@gmail.com).

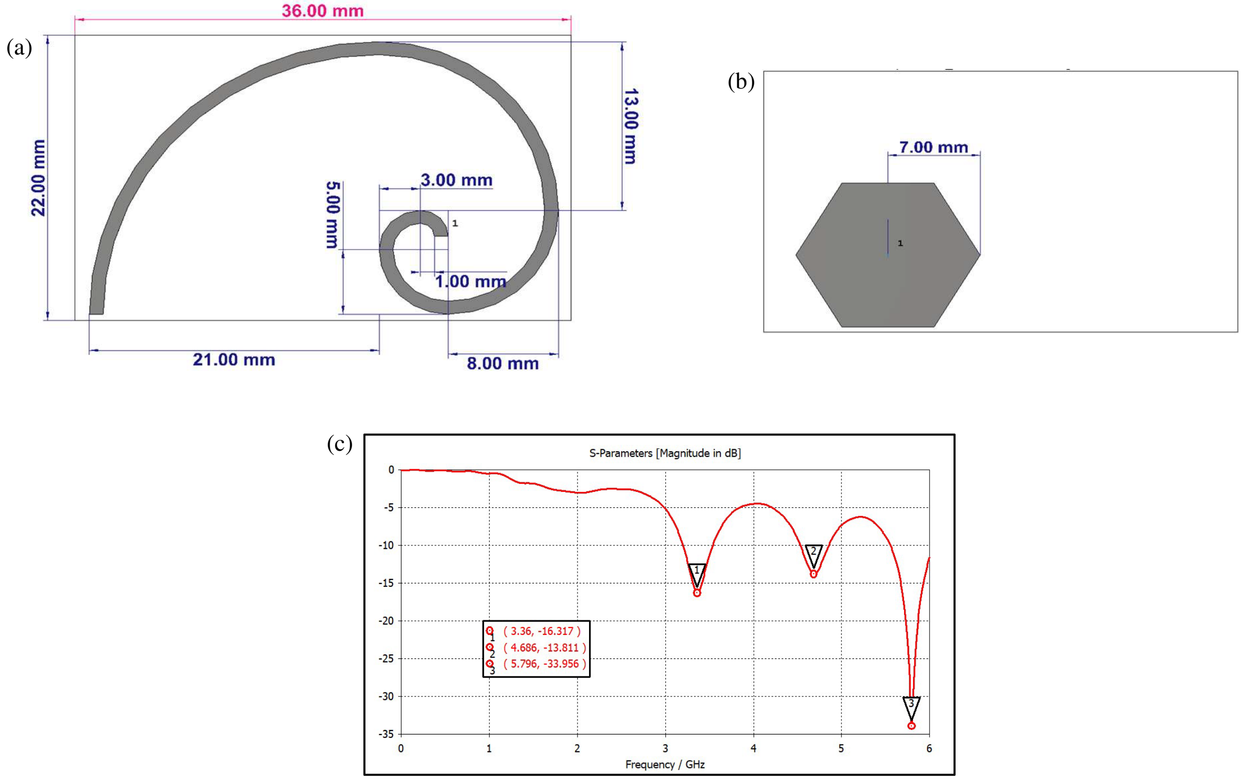

FIGURE 1. Single element Fibonacci antenna. (a) Single-element patch, (b) single-element ground plane, and (c) S_{11} of single element.

been examined for FR2 bands, showing that fractal concepts can scale to millimeter-wave frequencies [11, 14].

Between 2020 and 2021, significant steps were taken in compact fractal MIMO antennas with better isolation and diversity performance. Sunflower-inspired and ultra-wideband fractal MIMO antennas achieved low mutual coupling and reduced envelope correlation coefficient (ECC) [17, 19]. Experimental studies on compact fractal-based MIMO antennas for sub-6 GHz bands confirmed their suitability for new 5G systems [15, 16], validating fractal geometries as effective solutions for compact and multiband MIMO designs. Earlier efforts concentrated on techniques to reduce mutual coupling, such as defected ground structures, parasitic elements, and structural decoupling. These techniques became key enablers for compact MIMO setups [18–21]. Subsequently, fractal slot- and patch-based MIMO antennas were developed to support multiple wireless standards while improving the impedance bandwidth and miniaturization [22, 23]. Basic research has laid foundations for the theory and practice of MIMO antennas that were compact and manufactured using printed circuit board (PCB) technology, highlighting some basic problems associated with mutual coupling, correlation, and compactness [24, 25]. These developments set a foundation for further improvements in fractal and compact MIMO antennas. There is an evident gap in research for a simplified, scalable fractal geometry-based MIMO antenna system design that exhibits high isolation and low ECC, high radiation efficiency, and operates in multiple bands, including different 5G frequency bands.

The novelty of this work lies in:

- The first Fibonacci-inspired fractal geometry combined with slotted DGS for compact two-element MIMO antenna.
- Systematic design evolution from single element to optimized MIMO antennas.
- A comprehensive surface-current explanation of the coupling reduction mechanism.
- Complete experimental validation, including gain, efficiency, mean effective gain (MEG), total active reflection coefficient (TARC), radiation pattern, isolation, ECC, diversity gain (DG).

2. ANTENNA GEOMETRY AND DESIGN EVOLUTION

2.1. Single-Element Fibonacci Antenna

Figure 1 shows the geometry of the proposed single-element Fibonacci fractal antenna with a form factor of $36 \times 22\,\text{mm}^2$, comprising a spiral-like radiating patch and a small hexagonal ground plane. The simulations are carried out in Computer Simulation Technology (CST) Studio. The spiral geometry, inspired by the Fibonacci series, is designed on an FR4 substrate, selected for its self-similar and space-filling properties; hence, it will enable good miniaturization alongside multi-band and wideband electromagnetic performance. The spiraling radiating element slowly progresses in curvature in the Fibonacci series and therefore provides multiple effective current paths with different electrical lengths. Such an antenna ensures resonance at multiple frequencies without increasing its physical size. In addition, the spiral's smooth curve allows reduced current discontinuities, resulting in improved impedance matching and radiation stability. The spiral's inner section handles the high-frequency range while the outer section handles low frequencies, allowing for a larger frequency bandwidth. The hexagonal ground plane also increases antenna performance. The hexagon-shaped ground plane (7 mm each side) ensures uniform current distribution, which prevents edge diffraction and increases radiation efficiency compared to rectangular ground planes. Overall, the single-element Fibonacci antenna is able to achieve a good balance among size, increased bandwidth, and radiation stability, and hence can be used to form MIMO structures. The antenna exhibits three resonances at approximately 3.36 GHz, 4.66 GHz, and 5.8 GHz, with return losses of -16 dB, -13.8 dB, and -34 dB, respectively, and bandwidths of 352 MHz, 322 MHz, and 602 MHz.

2.2. Two-Element MIMO Fibonacci Antenna Evolution

Figure 2 represents the MIMO version designed during the first stage, where two identical Fibonacci spirals were combined with their corresponding hexagonal ground planes in one substrate. This design is useful for investigating mutual coupling and diversity when moving from a one-element to a multi-element antenna. As depicted in Figure 2(a), spirals are arranged in a mirror orientation at an optimized spacing to achieve compactness and isolation. This mirror structure results in surface currents flowing in opposite directions in each element after excitation, minimizing mutual coupling. Also, there will be minimal overlap in near fields in each element, hence less electromagnetic interaction. The solation is further improved by geometry of the Fibonacci spiral, which makes the surface currents decay rapidly within the excited element, reducing energy transfer to neighboring element without requiring additional structures for decoupling, such as neutralization lines and parasitic elements. Furthermore, using separate compact grounds instead of a single continuous ground plane helps suppress common-mode currents, which significantly contribute to mutual coupling in closely spaced MIMO arrays. This design choice significantly boosts isolation while preserving high radiation efficiency.

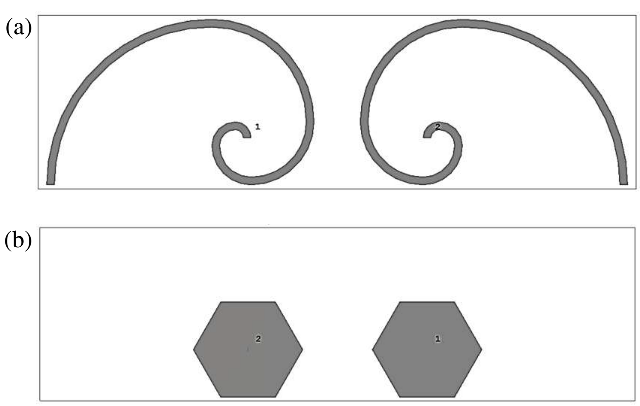

FIGURE 2. Two-element MIMO Fibonacci. (a) Front view and (b) ground plane.

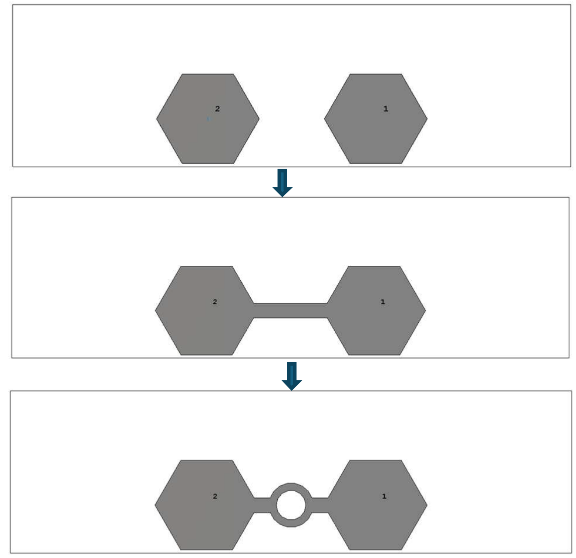

FIGURE 3. Modification in ground plane of MIMO.

Figure 3 illustrates changes in the ground plane design of the proposed Fibonacci MIMO antenna. Three stages of design development can be considered to resolve the problem of isolation and enhancement of antenna parameters. In the first stage of design development, two independent hexagonal ground planes are placed under each of antenna radiating elements with a physical gap between them. It is evident that, in terms of mutual coupling reduction, isolated ground planes are preferable to a common one, because there is no possibility for direct surface-current flow between the antenna elements. To solve problems associated with isolated grounds, a narrow rectangular conductive strip is added in the second design stage to connect two hexagonal ground planes. Such a change in the design affects the distribution of surface currents, creating additional current return paths. In addition, such a connecting strip has the function of equalization and phase balancing of induced currents, suppressing current concentration at the edges of the ground planes, which are the main source of coupling. In the final design, adding a circular slot at the center of the connecting strip results in a modified DGS. In this design, the advantages of the grounds' connection and the frequency-selective suppression of surface currents are combined. The circular slot serves as a band-stop filter for surface currents and breaks the main coupling path, but still ensures the controlled ground connection between the two antenna elements. This leads to redistributing surface currents near the slot, reducing their values close to the adjacent antenna element.

Figure 4 shows the process of modifying a compact two-element MIMO antenna system based on the Fibonacci spiral geometry. First, two symmetrical spirals are placed beside each other; these radiators serve as main MIMO elements. The second geometries have shapes similar to those of logarithmic/Fibonacci spirals, which are widely employed in antenna design because their self-similarity property provides broadband or multiband operation and current distribution improvement. Nevertheless, the proximity of mentioned structures results in significant electromagnetic coupling, reducing the per-

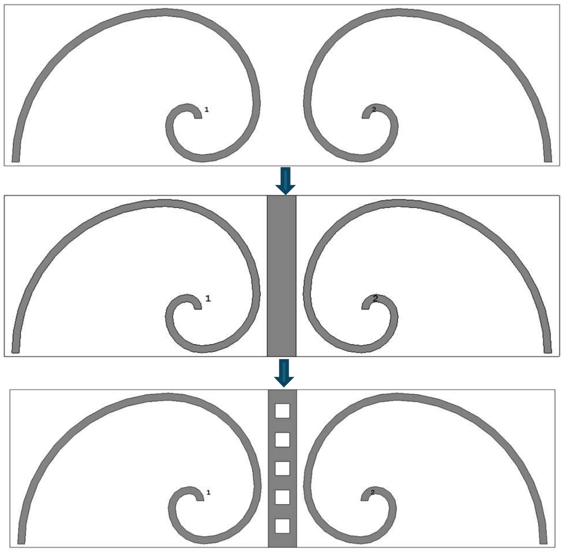

FIGURE 4. Modification in the MIMO patch.

formance of the MIMO antenna. Second, a vertical conductive strip is added between the two radiating elements. It serves as a decoupling or neutralization structure, changing the surface current flow paths and providing impedance between the antenna elements. Such an alteration helps reduce the coupling effect, usually evaluated through the S_{21} parameter, reducing electromagnetic coupling without enlarging antenna size and, hence, input impedance. Third, the central strip is modified by etching rectangular slots to create a defected structure. These notches generate more inductance and capacitance effects in the transmission path, generating a filter-like behavior or a band-stop response. This results in further suppressing surface waves from propagating through the coupling path, leading to increased isolation and good return loss (S_{11}). This stage represents an optimization step in which the electromagnetic behavior is finely tuned to achieve better MIMO performance metrics, such as the envelope correlation coefficient (ECC), diversity gain, and radiation efficiency, while maintaining a compact, structurally efficient antenna design.

Figure 5 shows the impact of design modifications on S_{11} and indirectly the mutual coupling behavior S_{21}, which is critical for MIMO performance. In the initial stage, the antenna elements operate with separate ground planes. This configuration exhibits relatively poor, inconsistent impedance matching across the band, with a very sharp resonance near 5.8 GHz. While such a deep notch indicates strong resonance, it is narrowband and unstable, and the lack of a shared ground leads to higher surface wave propagation and increased mutual coupling. This is generally undesirable in MIMO systems because it increases the correlation between antenna elements. When the grounds are connected, a common reference plane is established. This provides immense response stability and also improves matching at 1.1 and 3.3 GHz. This happens due to the more uniform redistribution of the return current in the unified ground, which eliminates impedance mismatching and undesired radiation mode. However, the coupling is still not fully controlled. Adding the ring caused a change in the current distribution. The ring serves as a resonant element,

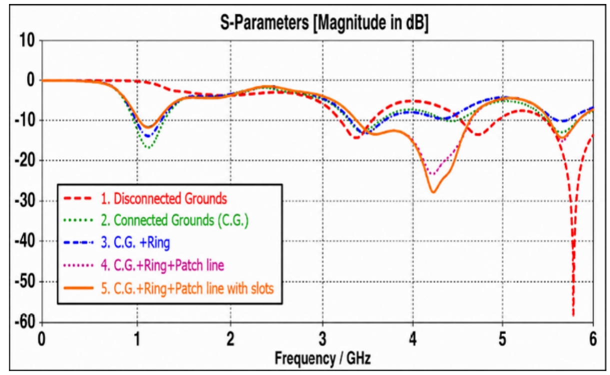

FIGURE 5. Parametric results of MIMO with modifications.

adding new channels for the current flow and coupling capacitance/inductance. Therefore, the response becomes smoother and wider, particularly in the mid-frequency range (3–5 GHz). It has a wider bandwidth and good control over the resonant modes. The resonances have a significant depth. In the fourth case, a parasitic element was added. It increases energy coupling into the radiating part and improves impedance matching, particularly at 4.1 GHz, where a pronounced resonance (-20 dB) occurs. The patch line is a good means of tuning the antenna, allowing alteration of its input impedance and phase response.

Finally, the optimized design is made defective by including slots in the patch/ground structure. These slots introduce additional inductive and capacitive effects that act as filters for the surface currents. This results in an order-of-magnitude higher and more controlled resonance (-27 dB at 4.22 GHz) and better matching over a larger band. The slots also disrupt surface wave propagation, reducing mutual coupling and enhancing isolation, which are key requirements for efficient MIMO operation.

2.3. Final Geometry Two-Element MIMO Fibonacci Antenna

Figure 6 illustrates the optimized geometry of the MIMO antenna system with a form factor in both its front and ground views. In the front view, two symmetrical Fibonacci-like spiral antennas were placed inside a small area of 76 mm × 22 mm. To reduce the mutual coupling and increase impedance matching, a middle slotted strip (4 mm) was inserted, serving as a decoupling structure. In the ground view, the DGS concept is applied, where hexagonal rings, along with a thin strip, connect through a circular ring. It plays a role in controlling current flow and suppressing surface waves, improving isolation and ensuring resonance.

Figure 7 depicts the reflection coefficient of a two-port antenna in the frequency range of 0 to 6 GHz, showing device performance in signal reflection. The reflection coefficient response shows three distinct resonant frequencies, approximately at 1.11, 4.22, and 5.65 GHz, with corresponding impedance bandwidths of 1–1.23 GHz, 3.34–4.60 GHz, and 5.52–5.76 GHz, respectively. The reflection coefficient values at these frequencies are around -11.89 dB, -27.22 dB, and -14.32 dB, respectively. This indicates that there is good

(a)
(b)
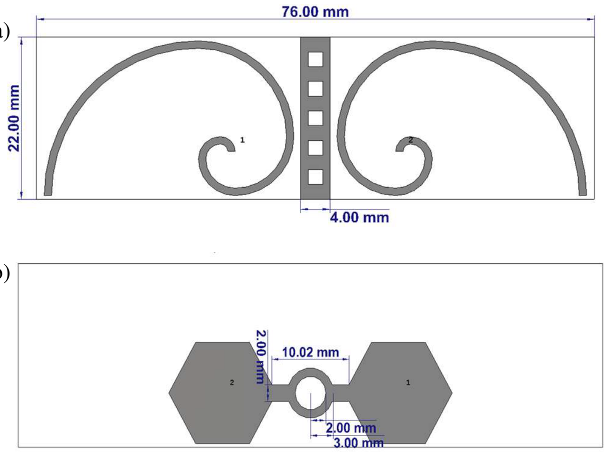

FIGURE 6. Final geometry of MIMO antenna. (a) Front view of MIMO and (b) ground view of MIMO.

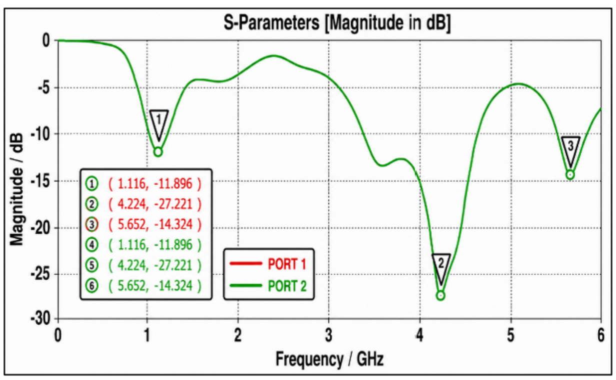

FIGURE 7. Reflection coefficient of the final MIMO antenna.

impedance matching at all three resonant frequencies. Among them, the 4.22 GHz resonant frequency has the lowest reflection coefficient value, -27.22 dB, indicating that it has the best impedance matching and also least reflected power. The other two resonant frequencies of 1.11 GHz and 5.65 GHz have acceptable matching, with reflection coefficient values of -11.89 dB and -14.32 dB, respectively.

The existence of several resonances proves that the antenna operates effectively in multiple frequencies, which is very important in modern-day wireless technology, as several wireless protocols have to be supported by a single antenna for communication purposes. The similarity between the S-parameter responses of both ports also suggests very little imbalance in the design, which is important to ensure minimum correlation and maximum diversity gain in MIMO systems. From the perspective of practical implementation, these operational frequencies would make the proposed antenna system feasible for use in several wireless communication applications. The low-frequency resonance demonstrates the multiband capability of the proposed geometry and may be suitable for narrowband L5-band applications. Primary operating bands are centered around 4.22 GHz and 5.65 GHz. For instance, the first band of 1.1 GHz can be considered for applications, such as L5-band (1176.45 MHz) communication, comprising systems such as GPS. The second frequency band, operating near 4.2 GHz, falls within the C-band. It links lower mid-band protocols [5G NR n77/n78, LTE 42/43 (3.30–3.80 GHz), and Wi-MAX (3.40–3.60 GHz)] to higher mid-band systems [5G NR n79, extended C-band, and specialized networks (4.40–4.99 GHz)]. This renders the band highly applicable to 5G, satellite, radar, and novel wireless communication systems.

Transmission coefficients S_{21} and S_{12} of the final MIMO antenna, shown in Figure 8, indicate good reciprocal behavior between antenna ports. The coupling is relatively high around 1–1.5 GHz, while above approximately 2.5 GHz, the transmission coefficient remains mostly below -15 dB, indicating **good isolation and reduced mutual coupling** between the antenna elements. Overall, the antenna shows satisfactory isolation at higher frequencies, which is beneficial for MIMO performance.

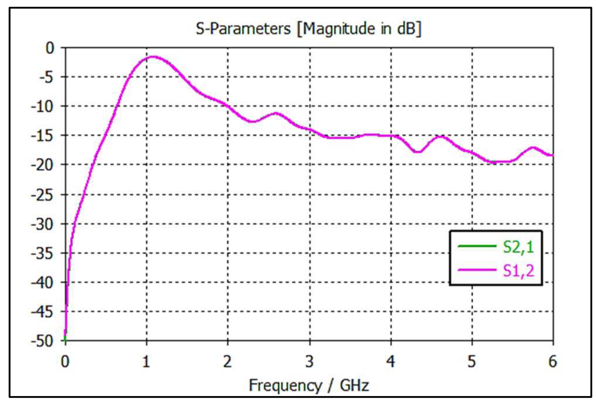

FIGURE 8. Transmission coefficient of the final MIMO antenna.

3. RESULT AND DISCUSSION

The antenna performance with respect to radiation characteristics is improved significantly, as observed in Figure 9, which illustrates gain improvement and generation of radiation lobes. At a frequency of 1.1 GHz, the antenna exhibits a fairly omnidirectional operation, and the 3D graph suggests a very uniform distribution of energy in nearly all directions. This trend is supported by the E- and H-plane graphs, and they exhibit nearly identical circular shapes.

The omnidirectional operation is a characteristic of electrically small antennas and is perfectly suited for covering large areas with IoT devices, Global System for Mobile Communication (GSM), or other communications in low-frequency bands. However, as the frequency increases to 3.5 and 4.22 GHz, the antenna performance is changed to a directed mode of operation. The lobes' elongated shape can be observed in 3D graphs, which indicates that the antenna is more focused on emitting its radiation in certain preferred directions. Although some lobes start to form in the E-plane cuts and are asymmetric in the H-plane plots, they are still relatively smooth and are perfect for 5G sub-6 GHz and Wi-MAX bands. Considering the improved value of 4.5 GHz, the radiation pattern now depicts a dominant, clear main lobe with controlled side lobes, contrary to the previous one that had no clear dominant main lobe and was unstable and fragmented. The plot shows that the radiation from the antenna at 4.5 GHz is more stable and consistent because the

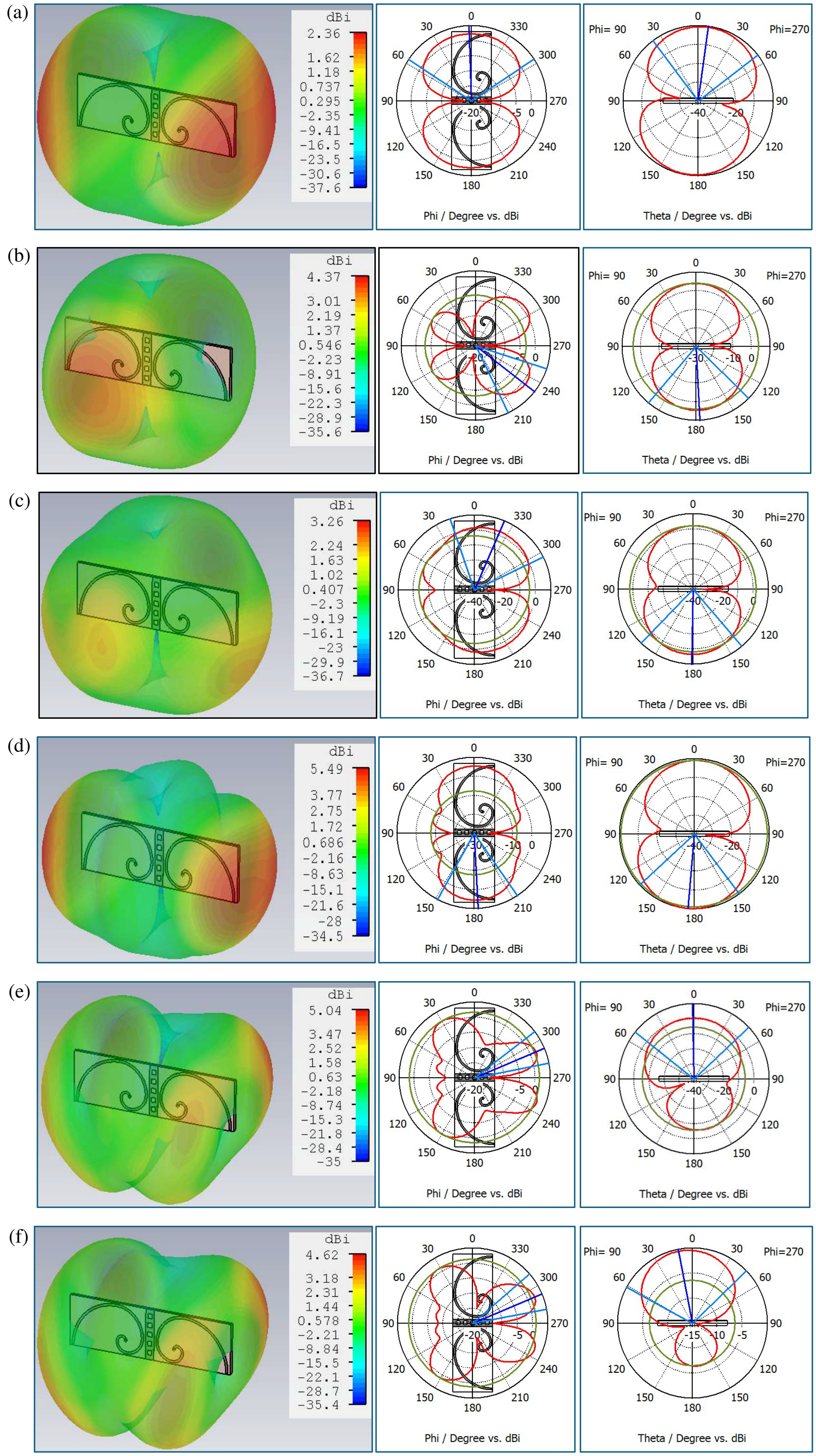

FIGURE 9. 3D and 2D (E-plane and H-plane) radiation pattern of the antenna. (a) 1.1 GHz, (b) 3.5 GHz, (c) 4.23 GHz, (d) 4.5 GHz, (e) 5.65 GHz, and (f) 5.8 GHz.

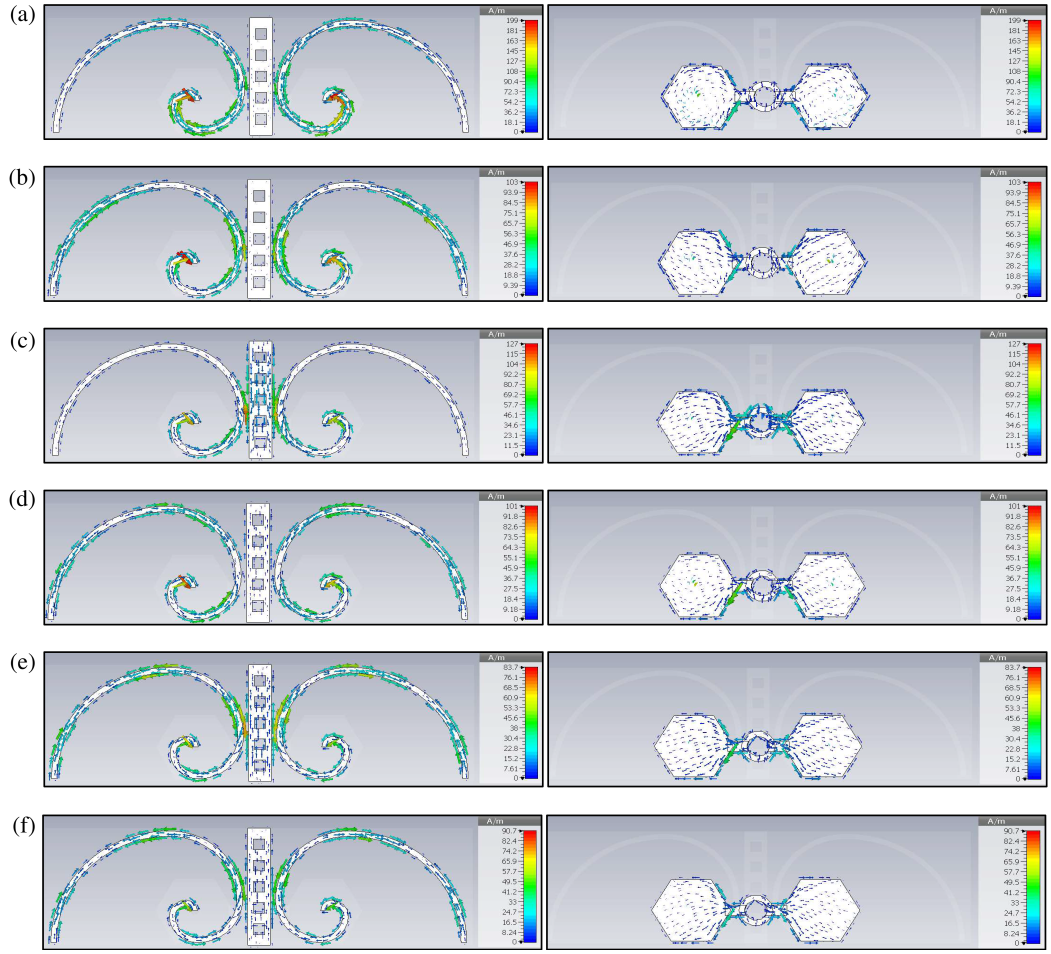

FIGURE 10. Surface current distribution of the antenna. (a) 1.1 GHz, (b) 3.5 GHz, (c) 4.23 GHz, (d) 4.5 GHz, (e) 5.65 GHz, and (f) 5.8 GHz.

radiation beam appears stable. In the E-plane, there is symmetry and stability in the lobes, whereas the H-plane shows relatively stable directionality. This improvement confirms the antenna's resonating nature at 4.5 GHz, and hence it is ideal for point-to-point communications, WLAN, or mid-band 5G applications. The antenna, at a frequency of 5.65 GHz, shows radiation complexity with the development of multiple lobes in the 3D plot because of the excitation of higher-order modes. However, compared to previous measurements, this antenna shows a dominant radiation direction with side lobes present. In the E-plane, there is a sharp variation and deep nulls, whereas in the H-plane, there is more irregularity. Therefore, although the antenna can provide high-gain radiation in one direction, there can be unwanted radiation in other directions. This type of radiation can therefore be useful in systems such as WLAN (5.8 GHz), radar technology, and short-range high-data-rate communications. In short, new results clearly reveal the dependence of the antenna's radiation characteristics on frequency, starting from the radiation of an omnidirectional nature to highly directive radiation in medium and high-frequency bands. The improved results at 4.5 GHz confirm the presence of an efficient radiation mode, which forms the basis of the antenna operation and thus its validity for multiband communication systems.

Figure 10 depicts the multiband characteristics of surface current distributions of the proposed Fibonacci MIMO antenna with respect to the radiation patch and defected ground plane at different resonant frequencies. At 1.17 GHz, the current distribution is predominantly on the inner spiral arms and feeding region, implying that the fundamental resonant mode is excited by an increase in the current path. For 3.5 and 4.23 GHz, the current distribution covers large areas of the spiral structure and its curved parts, implying that higher-order modes are being excited. Additionally, there is a notable current distribution on the ground plane within the center defected region, signifying its involvement in impedance matching and reduced coupling effect. In the case of 4.5 GHz, there is a symmetrical current distribution with several peaks of maximum current distribution on the spiral edges, implying improved isolation performance of the MIMO antennas. At 5.65 and 5.8 GHz, the surface-current distribution is predominant in the spiral's outer part and feed regions because of the short resonant current path. Overall, based on the results of the surface current analysis, it was confirmed that the Fibonacci spiral shape with the defected ground structure helps achieve multiband resonance, better isolation, and stable radiation performance in wireless communications.

Figure 11 presents the Envelope Correlation Coefficient (ECC) of the MIMO antenna design across the operating

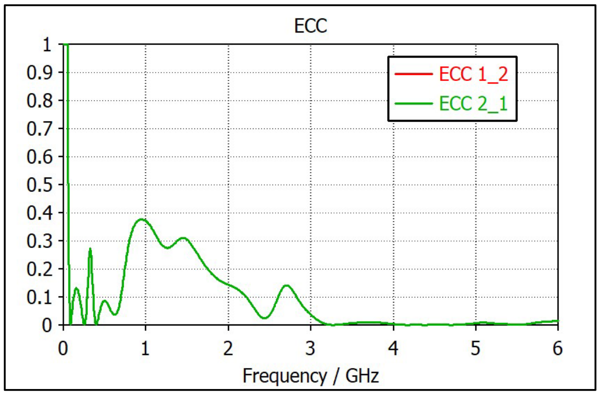

FIGURE 11. ECC of the antenna.

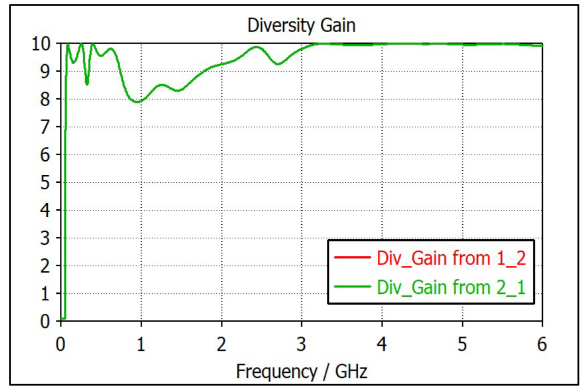

FIGURE 12. Diversity gain of the antenna.

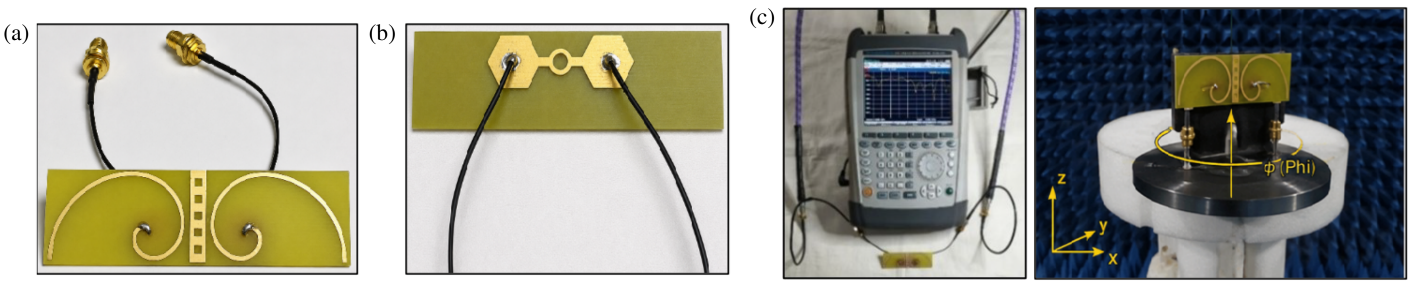

FIGURE 13. Fabricated prototype with measurement setup. (a) Patch, (b) ground plane, and (c) antenna with measurement setup.

bandwidth. The ECC of the antenna elements has been very low across almost all band ranges and tends towards zero for the band range above 3 GHz. There are a few fluctuations in the ECC value at lower frequencies; nevertheless, the ECC remains within an acceptable range (< 0.5).

Figure 12 shows the diversity gain (DG) performance of the new antenna. The antenna's diversity gain is near its ideal level of 10 dB throughout most of the working frequency range. There are slight variations in diversity gain levels in the lower-frequency range, but it quickly attains stable values at higher frequencies. This indicates that the antenna is suitable for MIMO systems due to its high diversity gain and ECC values.

4. FABRICATED STRUCTURE AND VALIDATION OF RESULTS

Figure 13 depicts the fabricated prototype model of the developed Fibonacci MIMO antenna along with its experimental measurement setup. Figure 13(a) displays the front view of the fabricated antenna patch where the Fibonacci spirals serving as the antenna's radiating elements are engraved onto the substrate. They are further connected using SMA connectors for exciting the signal into the antenna. Figure 13(b) shows the defected ground-plane structure of the antenna, which is placed on the back side of the fabricated antenna. This defected ground structure improves the impedance matching capability of the proposed antenna design and reduces the undesired mutual coupling effect between the elements of the proposed antenna. Figure 13(c) depicts the antenna's experimental measurement setup.

The antenna's fabricated prototype was characterized using a Vector Network Analyzer (VNA-R&S ZVH 8) to determine the antenna's reflection coefficients and impedance characteristics. The radiation pattern and gain characteristics were determined in an anechoic chamber, in which the antenna was fixed on a rotating mount to determine the radiation characteristics at different angles in φ and θ planes.

Figure 14 represents a comparison between simulated and measured reflection coefficients (S_{11}/S_{22}) of the proposed Fibonacci MIMO antenna in the working frequency band. As shown in Figure 14, the measured values coincide with the simulation result, which indicates the accuracy of the design, as well as the manufacturing process. Three resonance bands are observable in the reflection coefficient plot where the reflection coefficient value is less than -10 dB, suggesting efficient antenna operation due to impedance matching. The highest resonance band occurs at 4.22 GHz, where the reflection coefficient in the simulation result is -27 dB. However, the measured reflection coefficient is a little bit higher than the simulated value due to a number of reasons, including tolerances in antenna manufacture, SMA connector loss, soldering effects, and measurement errors. Some deviations in the frequency value and resonance depth are also visible in both the reflection coefficient plots. Nevertheless, the minor difference between values does not change the fact that the data measured are in line with the simulation for all working frequency ranges. Hence, the reflection coefficient proves the antenna's multi-band nature for

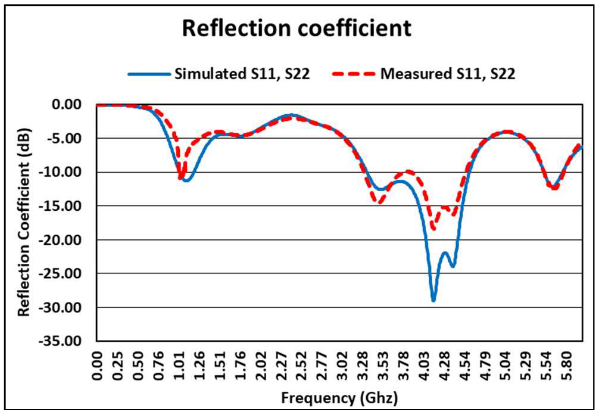

FIGURE 14. Comparison of simulated vs measured reflection coefficients.

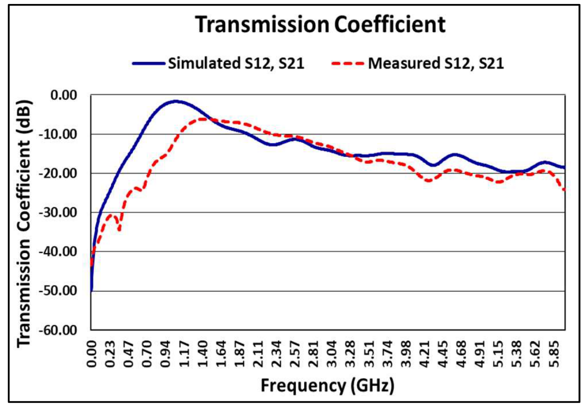

FIGURE 15. Comparison of simulated vs measured transmission coefficients.

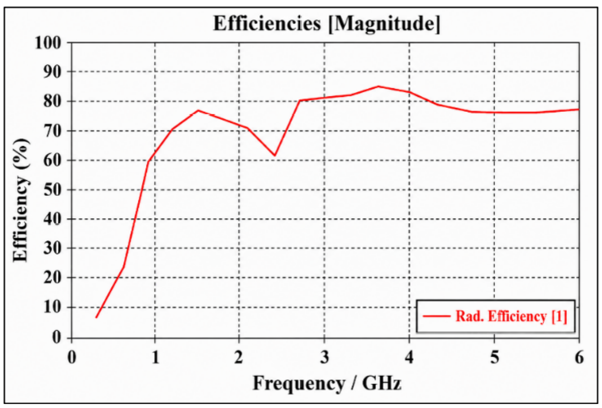

FIGURE 16. Radiation efficiency of antenna.

wireless communications, such as Wi-MAX, WLAN, and sub-6 GHz 5G bands.

Figure 15 shows the simulation and measurement of transmission coefficients (S_{12} and S_{21}) and mutual coupling of radiating elements. The results of simulation and experiments show the same tendency, proving the efficiency of the isolation method. In the low-frequency range, the transmission coefficient remains below -30 dB showing the efficient isolation of the antennas from each other. The increase in coupling occurs between 1 and 1.3 GHz, but then transmission coefficients start decreasing and remain below the -15 dB threshold for the entire operating frequency range. At high frequencies, the isolation becomes less than -20 dB according to the experimental results. The findings above show that the proposed MIMO antenna guarantees proper isolation and diversity.

The efficiency chart illustrates (Figure 16) radiation efficiency variations of the designed antenna with frequency. Radiation efficiency increases rapidly with increasing frequency, mostly in the range of 75% to 85% in the upper operating frequencies. These results suggest that there are some losses from radiation and efficient transmission of the electrical power. It can be noted that there is a substantial increase in efficiency values at frequencies beyond 3 GHz, which may be due to the efficient matching of impedance and minimized losses in dielectric and conductive materials at these higher frequencies. Increased radiation efficiency for frequencies higher than 3 GHz implies that more input power is efficiently radiated. Some fluctuations in efficiency occur because of impedance mismatch and losses associated with the dielectric material at some frequencies.

Figure 17 compares simulated and measured radiation patterns of the proposed multiple-input multiple-output (MIMO) antenna at 1.1, 3.5, 4.2, 4.5, 5.65, and 5.8 GHz. The measured radiation patterns were in good agreement with simulated results in the direction of the main lobe and overall radiation characteristics. At 1.1 GHz, the antenna presents a bidirectional radiation pattern, with main lobes that are almost identical in simulation and measurement. The characteristic butterfly-shaped pattern is retained at 3.5 GHz, with only small variations in null depth and side-lobe levels. The measured patterns at 4.2 and 4.5 GHz match the simulated broadside radiation with small variations in the lobe amplitudes. At the upper frequencies of 5.6 and 5.8 GHz, the antenna shows stable radiation performance, and good agreement is observed between simulated and measured results. However, slight beam broadening and asymmetry are observed in measured patterns. Small differences between simulated and measured radiation patterns are attributed to fabrication tolerances, variations of the dielectric constant and loss tangent of the FR-4 substrate, connector and SMA soldering effects, cable radiation during measurement, chamber alignment errors, and environmental reflections in the measurement setup. Nevertheless, the measured results follow the simulated characteristics very well, despite these practical limitations, which proves that the proposed antenna achieves stable radiation performance over the entire operating band. The close agreement between the simulated and measured results validates the antenna design, confirming its suitability for sub-6 GHz 5G and WLAN MIMO applications.

Figure 18 presents simulated and measured Mean Effective Gains (MEGs) of the two antenna elements over the operational frequency range. The measured characteristics of MEG-1 and MEG-2 are in good agreement with the simulated results over the whole operating band. The two antenna elements display nearly identical MEG characteristics, indicating balanced power reception and symmetrical radiation performance within

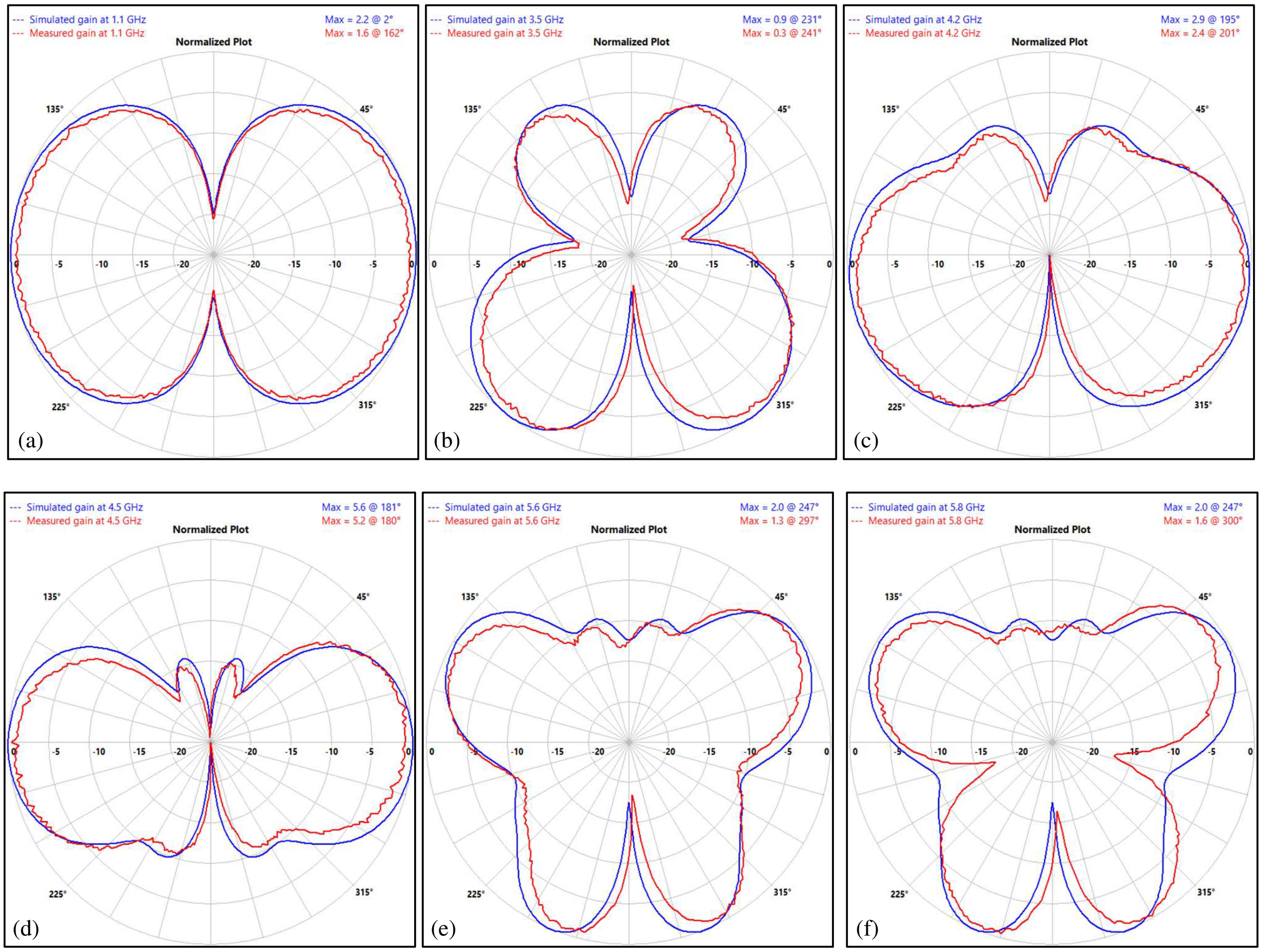

FIGURE 17. Measured vs simulated gain. (a) Gain at 1.1 GHz, (b) gain at 3.5 GHz, (c) gain at 4.22 GHz, (d) gain at 4.5 GHz, (e) gain at 5.65 GHz, and (f) gain at 5.8 GHz.

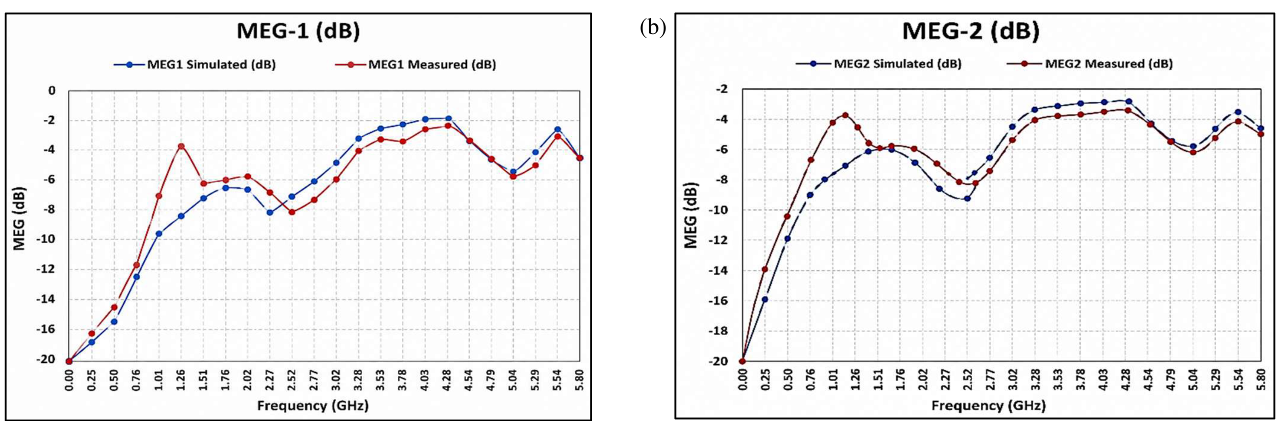

FIGURE 18. Measured vs simulated MEG. (a) MEG-1 and (b) MEG-2.

a uniform multipath propagation environment. The MEG values are close to -3 dB for most operating frequencies, which is the desired value for a well-balanced two-port MIMO antenna. This indicates that the two antenna elements receive almost the same amount of incident power and contribute equally to overall MIMO system performance. Therefore, the proposed antenna satisfies the MEG requirement for sub-6 GHz, 5G, and WLAN MIMO applications.

Figure 19 illustrates the comparison of simulated and measured Total Active Reflection Coefficients (TARCs) of the proposed two-port multiple-input multiple-output (MIMO) antenna across the operational frequency range. The measured

TABLE 1. Comparative analysis.

Ref.	Structure Shape	No. of Elements	Resonant Bands/ Frequencies	Operating Bands	No. of Bands	Peak Gain (dBi)	Efficiency	ECC	Diversity Gain
Proposed work	Fibonacci shaped with DGS	2	1.1 GHz, 4.2 GHz, 5.66 GHz	L-band (L5), Wi-MAX, WLAN/Wi-Fi, 5G n78/n79	Tri-band	5.49	75–85%	< 0.05	> 9.95 dB
[1]	Fractal Hilbert MIMO	2	3.5 GHz, 4.8 GHz	Sub-6 GHz 5G	Dual-band	4.5	80%	< 0.05	> 9 dB
[2]	Fractal Hilbert MIMO	4	6 GHz	Wi-Fi 7, Wi-Fi 8, and 5G sub-6 GHz	Single	5.47	82%	< 0.04	> 9.8 dB
[4]	Miniaturized DGS MIMO	2	∼2.4 GHz, 3.5 GHz, 5.2 GHz	Future mobile bands	Tri-band	5.2	82–88%	< 0.04	9.8 dB
[9]	Fractal UWB-MIMO	2	3.1–10.6 GHz	UWB	UWB	5.1	85–90%	< 0.05	9.7 dB
[11]	Minkowski fractal MIMO	2	24 GHz, 28 GHz, 38 GHz	FR2 5G	Tri-band	7.8	87–92%	< 0.03	9.9 dB
[12]	Quasi-fractal DGS antenna	2	∼2.4 GHz, 3.5 GHz, 5.5 GHz	Multiband wireless	Tri-band	5.9	88%	< 0.04	9.8 dB
[15]	Fractal-based MIMO	2	3.5 GHz, 4.8 GHz	Lower sub-6 GHz 5G	Dual-band	5.4	86%	< 0.05	9.6 dB
[18]	Compact MIMO with coupling reduction	2	∼2.4 GHz, 5.0 GHz	Wireless bands	Dual-band	5.0	85%	< 0.05	9.5 dB

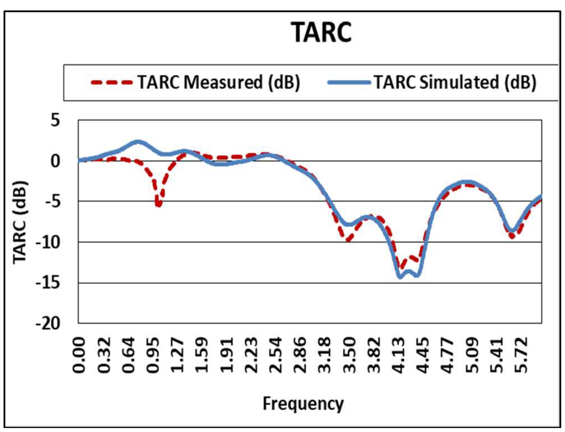

FIGURE 19. TARC.

TARC characteristics exhibit strong agreement with the simulated profiles over the entire operational band.

The proposed antenna exhibits multiple resonance regions with low TARC values, showing effective active impedance matching when both ports are excited simultaneously. The lowest TARC minimum occurs within the 4.3–4.5 GHz range with a magnitude of -14 dB, indicating a significant drop in reflected power during simultaneous port excitation. Additional TARC minima are observed near 3.5 and 5.6 GHz, aligning with the antenna's primary target operational bands. The low TARC levels for all operating ranges indicate that the design successfully minimizes active reflection and coupling between the radiator elements. These results validate the efficient power transfer and excitation in the real world. Therefore, the excellent correlation between numerical and experimental TARC levels proves the antenna's suitability for MIMO use.

5. COMPARATIVE STUDY WITH LITERATURE

A comparative study of recently reported fractal and miniaturized MIMO antennas in Table 1 demonstrates the use of basic fractals, such as Hilbert, Minkowski, Koch, Sunflower, and slot antennas. Such antennas have a primary goal of achieving compactness, good isolation, low ECC, and diversity performance for 5G, WLAN, and Wi-Fi communications. In contrast, the designed Fibonacci MIMO antenna utilizes a unique fractal structure inspired by the Fibonacci series, which improves current distribution and electromagnetic coupling management. It allows the antenna to provide compactness and ensure stable radiation properties in various bands. While some recent designs achieve higher gains and broader bandwidths, many antennas need large sizes, parasitic structures, or multilayer configurations. The designed Fibonacci MIMO antenna is aimed at providing structural simplicity, sufficient gain, isolation, low ECC, radiation efficiency, and confirmed multi-band functionality.

Hence, the proposed structure provides a reasonable compromise between compactness, performance, and fabrication simplicity.

6. LIMITATIONS OF PROPOSED ANTENNA

Although the presented design has good performance for multiband operation and good MIMO properties, it has certain drawbacks. In low-frequency resonance, the impedance bandwidth is not very wide, and therefore this resonator is more suitable for narrowband than for broadband GPS operations. The same applies to impedance matching at 5.65 GHz. Compared to other recently published fractal MIMO antennas, this one has an average gain and radiation efficiency.

7. CONCLUSION

An optimized, miniaturized, Fibonacci-inspired two-element MIMO antenna with an improved DGS (defected ground structure) design has been developed, prototyped, and extensively analyzed. Such an antenna uses the self-similarity of the Fibonacci spiral geometry to facilitate multiband operation while minimizing antenna size. Optimal design of the radiating element and ground plane results in excellent impedance matching, isolation, and diversity. The proposed antenna operates efficiently at the resonant frequencies of 1.1 GHz, 4.22 GHz, and 5.65 GHz. The high accuracy of simulations and measurements proves the validity of the proposed design. Impedance matching is accomplished with a minimum reflection coefficient of -27.22 dB at 4.22 GHz frequency. Also, using the modified DGS helps decrease the effects of mutual coupling by ensuring isolation higher than 20 dB in all frequency bands. The MIMO performance of the proposed antenna is proved by an envelope correlation coefficient lower than 0.05 and a diversity gain greater than 9.95 dB. High-diversity performance is provided by this antenna in spite of its small dimensions and also results in a radiation efficiency higher than 75% and 85% at the maximum gain of 5.49 dBi. Overall, the novel MIMO antenna based on the Fibonacci sequence has an optimal combination of size, high isolation, low correlation, constant gain performance, and highly efficient radiation. All of these attributes make it a suitable candidate for sub-6 GHz 5G, WLAN, Wi-Fi, and Wi-MAX. The simplicity, compactness, and economy of the proposed antenna show the design's future potential to be implemented in next-generation multi-band wireless communication systems.

REFERENCES

[1] Jat, N., A. Kumar, E. M. Ali, M. Gupta, D. H. Elkamchouchi, and A. Nanthaamornphong, "Enhanced isolation unique fractal diminutive MIMO antenna with identical elliptical notch and cross stub for wireless uses," *Scientific Reports*, Vol. 15, No. 1, 36600, 2025.

[2] Sindhuja, N. M. M., R. Sreelakshmy, O. P. Kumar, and M. Raveendra, "Design of a Hilbert curve fractal MIMO slot antenna with enhanced bandwidth and stable radiation patterns for Wi-Fi 7 and Wi-Fi 8 applications using genetic algorithm," *International Journal of Antennas and Propagation*, Vol. 2026, No. 1, 8112380, 2026.

[3] Jahanbakhsh Basherlou, H., N. O. Parchin, and C. H. See, "A compact fractal-based super-wideband mmWave MIMO antenna for 5G NR and 6G services," *Electronics*, Vol. 15, No. 12, 2564, 2026.

[4] Kamil, N. R., A. G. Waddy, and A. H. Al-Nakkash, "A design of fractal Hilbert MIMO antenna for 5G mobile," *Journal of Techniques*, Vol. 4, No. 1, 29–38, Mar. 2022.

[5] Prasad, G. G. and G. S. Kumar, "Design of multiband miniaturized MIMO antenna with defected ground for future mobile communications," *Indian Journal of Engineering and Materials Sciences (IJEMS)*, Vol. 31, No. 6, 864–887, 2024.

[6] Khade, S. S., V. G. Girhepunje, S. S. Kurumbanshi, D. B. Bhoyar, J. D. Kene, A. R. B. Patil, S. K. Mohod, and S. Prayagi, "Advanced miniaturised MIMO architecture: High-isolation four-element antenna system for next-generation wireless connectivity," *African Journal of Applied Research*, Vol. 11, No. 6, 36–50, Nov. 2025.

[7] Khade, S. S., N. Mangrulkar, C. S. Khade, S. Dhanvijay, and P. L. Zade, "A dual-band four-element MIMO antenna with triangular slots and hexagonal rings for GSM, Wi-Fi, LTE, 5G and IoT applications," *Progress In Electromagnetics Research C*, Vol. 162, 70–80, 2025.

[8] Sidhu, A. K. and J. S. Sivia, "Design of wideband fractal MIMO antenna using Minkowski and Koch hybrid curves on half octagonal radiating patch with high isolation and gain for 5G applications," *Advanced Electromagnetics*, Vol. 12, No. 1, 58–69, Mar. 2023.

[9] Punna, B., M. Sofiyan, N. S. Reddy, and B. Nagarani, "Fractal-based UWB-MIMO antenna with reconfigurable band-notching characteristics," *Telecommunications and Radio Engineering*, Vol. 83, No. 8, 47–55, 2024.

[10] Khade, S. S., D. B. Bhoyar, K. Kotpalliwar, C. V. Bawankar, and M. S. Kimmatkar, "Four element EC slot MIMO antenna for WLAN, Wi-Fi and 5G applications," *Progress In Electromagnetics Research C*, Vol. 139, 147–158, 2024.

[11] Udeze, N. P., S. I. Orakwue, and M. I. Ehikhamenle, "Design of a tri-band Minkowski fractal MIMO antenna for FR2 5G applications," *Journal of Engineering Research and Reports*, Vol. 26, No. 9, 190–205, Sep. 2024.

[12] Rizvi, S. N. R., M. A. Sufian, N. Hussain, Y. Chun, S.-G. Park, S. Kim, and N. Kim, "Isolation enhancement of a capacitively-fed MIMO antenna using a quasi-fractal parasitic element and defected ground structure," *Heliyon*, Vol. 10, No. 20, e39228, Oct. 2024.

[13] Addepalli, T., M. S. Kumar, C. R. Jetti, N. K. Gollamudi, B. K. Kumar, and J. Kulkarni, "Fractal loaded, novel, and compact two-and eight-element high diversity MIMO antenna for 5G sub-6 GHz (N77/N78 and N79) and WLAN applications, verified with TCM analysis," *Electronics*, Vol. 12, No. 4, 952, 2023.

[14] Bisht, N., P. K. Malik, S. Das, T. Islam, S. Asha, and M. Alathbah, "Design of a modified MIMO antenna based on tweaked spherical fractal geometry for 5G new radio (NR) band N258 (24.25–27.25 GHz) applications," *Fractal and Fractional*, Vol. 7, No. 10, 718, 2023.

[15] Sree, G. N. J. and S. Nelaturi, "Design and experimental verification of fractal based MIMO antenna for lower sub 6-GHz 5G applications," *AEU — International Journal of Electronics and Communications*, Vol. 137, 153797, 2021.

[16] Gocen, C., "A compact DGS-assisted Koch-fractal U-slot MIMO antenna for sub-6 GHz 5G and WLAN applications," *Telecom*, Vol. 7, No. 4, 105, 2026.

[17] Abed, A. T., "Novel sunflower MIMO fractal antenna with low mutual coupling and dual wide operating bands," *International Journal of Microwave and Wireless Technologies*, Vol. 12, No. 4, 323–331, 2020.

[18] Islam, T., F. Alsaleem, F. N. Alsunaydih, and K. Alhassoon, "Mutual coupling reduction in compact MIMO antenna operating on 28 GHz by using novel decoupling structure," *Micromachines*, Vol. 14, No. 11, 2065, 2023.

[19] Singhal, S., "Four element ultra-wideband fractal multiple-input multiple-output antenna," *Microwave and Optical Technology Letters*, Vol. 61, No. 12, 2811–2818, 2019.

[20] Nejdi, I. H., S. Bri, M. Marzouk, S. Ahmad, Y. Rhazi, M. Ait Lafkih, Y. A. Sheikh, A. Ghaffar, and M. Hussein, "UWB circular fractal antenna with high gain for telecommunication applications," *Sensors*, Vol. 23, No. 8, 4172, 2023.

[21] Qin, Y., R. Li, and Y. Cui, "Embeddable structure for reducing mutual coupling in massive MIMO antennas," *IEEE Access*, Vol. 8, 195 102–195 112, 2020.

[22] Abed, A. T. and A. M. Jawad, "Compact size MIMO fractal slot antenna for 3G, LTE (4G), WLAN, WiMAX, ISM and 5G communications," *IEEE Access*, Vol. 7, 125 542–125 551, 2019.

[23] Huang, H., X. Li, and Y. Liu, "A low-profile, dual-polarized patch antenna for 5G MIMO application," *IEEE Transactions on Antennas and Propagation*, Vol. 67, No. 2, 1275–1279, Feb. 2019.

[24] Sharawi, M. S., "Printed multi-band MIMO antenna systems and their performance metrics [wireless corner]," *IEEE Antennas and Propagation Magazine*, Vol. 55, No. 5, 218–232, Oct. 2013.

[25] Kumar, A., G. Singh, M. K. Abdulhameed, S. R. Hashim, and A. J. A. Al-Gburi, "Development of fractal 5G MIMO antenna for sub 6 GHz wireless automotive applications," *Progress In Electromagnetics Research M*, Vol. 130, 121–128, 2024.